KSABC
The Korean Society for Applied Biological Chemistry

ARTICLE

Open Access

Anti-inflammatory components isolated from *Atractylodes macrocephala* in LPS-induced RAW264.7 macrophages and BV2 microglial cells

Hong-Guang Jin[1,2†], Kwan-Woo Kim[1,4†], Jing Li[1,3†], Dae Young Lee[4], Dahye Yoon[4], Jin Tae Jeong[4], Geum-Soog Kim[4], Hyuncheol Oh[1], Ren-Bo An[5*] and Youn-Chul Kim[1*]

Abstract

The phytochemical investigation on the methanol extract of the rhizomes of *Atractylodes macrocephala* resulted in the discovery of one new compound 9α-hydroxyatractylenolide (**1**) and 21 known compounds including atractylone (**2**), 3β-acetoxyatractylon (**3**), atractylenolide I (**4**), atractylenolide II (**5**), 8-epiasterolid (6), atractylenolide III (**7**), atractylenolide VII (**8**), 8-epiatractylenolide III (**9**), eudesm-4(15)-ene-7α,11-diol (**10**), linoleic acid (**11**), myristic acid (**12**), 3-*O*-caffeoyl-1-methyquinic acid (**13**), (2*E*,8*E*,10*E*)-tetradecatriene-4,6-diyne-1,14-diol (**14**), 14-aceroxy-12-senecioyloxytetradeca-2*E*,8*Z*,10*E*-trien-4,6-diyn-1-ol (**15**), isoscopoletin (**16**), caffeic acid (**17**), protocatechic acid (**18**), 3-*O*-caffeoylquinic acid (**19**), 4-*O*-caffeoylquinic acid (**20**), 1,5-di-*O*-caffeoylquinic acid (**21**), and nicotinic acid (**22**). Their structures were identified using nuclear magnetic resonance (NMR) and mass spectroscopy, and by comparison with previously published data. Compounds **4**, **5**, **6**, **8**, and **10**–**22** significantly inhibited lipopolysaccharide (LPS)-induced nitric oxide (NO) production in RAW264.7 macrophages, and compounds **4**, **5**, **6**, **16**, and **17** showed those responses in BV2 microglial cells. Especially, compound **6** showed the second-best effect, and inhibited the LPS-induced production of prostaglandin E2 (PGE$_2$), the protein expression of inducible nitric oxide synthase (iNOS) and cyclooxygenase (COX)-2, and the production of cytokines including interleukin (IL)-1β, IL-6, and tumor necrosis factor (TNF)-α in both cells. These inhibitory effects were mediated by the inactivation of nuclear factor kappa B (NF-κB) signaling pathway.

Keywords: Atractylodes macrocephala, Anti-inflammatory effect, Macrophages, Microglia, Nuclear factor kappa B

Introduction

Inflammation is associated with the activation of macrophages or monocytes that are responsible for the innate and adaptive immune responses of the human body.

Following various stimuli, these immune cells release a series of pro-inflammatory mediators including nitric oxide (NO), prostaglandin E2 (PGE$_2$), cytokines such as interleukin (IL)-1β, IL-6, and tumor necrosis factor (TNF)-α, chemokines, and signaling-associated proteins [1] to protect the infected tissues site and to maintain the homeostasis of the body [2]. However, a dysregulation of the inflammatory responses via continuous stimulation results in the overproduction of pro-inflammatory mediators, leading to the development of various inflammatory diseases including atherosclerosis, cardiovascular disorders, diabetes, tumor, asthma, septic complications,

*Correspondence: anrb@ybu.edu.cn; yckim@wku.ac.kr
†Hong-Guang Jin, Kwan-Woo Kim and Jing Li contributed equally to this work
[1] Institute of Pharmaceutical Research and Development, College of Pharmacy, Wonkwang University, Iksan 54538, Republic of Korea
[5] College of Pharmacy, Yanbian University, Yanji 133002, Jilin, People's Republic of China
Full list of author information is available at the end of the article

Jin *et al. Applied Biological Chemistry*   (2022) 65:11

Page 2 of 13

and neurodegenerative diseases [3–5]. Macrophages are the most dominant and widely distributed immune cell types throughout the body, and microglia are considered resident macrophages in the central nervous system (CNS) [6]. Macrophages and microglia are important sources of pro-inflammatory mediators through the activation of transcription factors such as nuclear factor kappa-light-chain-enhancer of activated B cells (NF-κB) and mitogen-activated protein kinase (MAPK) due to lipopolysaccharide (LPS) stimulation [7, 8]. LPS is the most abundant lipidic component of the gram-negative bacterial cell wall [9]. Since macrophages and microglia stimulated by LPS produce excessive pro-inflammatory mediators, they are being utilized in in vitro models to evaluate the effectiveness of potentially anti-inflammatory candidate substances [10, 11].

Atractylodes macrocephala, which belongs to the Compositae family, is a perennial herb, widely distributed in East Asia [12]. Traditionally, this plant has been used for the treatment of an abnormal function of the digestive system including malfunction of the spleen, anorexia, abdominal distension, diarrhea, dizziness, and palpitation due to the retention of phlegm and fluid, edema, spontaneous sweating, threatened abortion, oedema, excessive perspiration, and an abnormal fetal movement [13, 14]. In several recent studies, various components of *A. macrocephala* were isolated including essential oils, sesquiterpenoids, polysaccharides, amino acids, vitamins, and resins [15], and their physiological activity including anti-inflammatory [16], neuroprotective [17], anti-cancer [18], anti-oxidant [19], and immunological enhancement effects [20] were evaluated. In this investigation, we described the isolation and structural identification of 22 compounds from the rhizomes of *A. macrocephala* together with the evaluation of their anti-inflammatory effects using RAW264.7 macrophage and BV2 microglial cell lines.

Materials and methods
Plant materials
The rhizomes of *A. macrocephala* were harvested in Andong (Gyeongbuk) in December 2018. The plant material was identified by Prof. Youn-Chul Kim, College of Pharmacy, Wonkwang University, Iksan, Korea. A specimen of *A. macrocephala* (No. WSY-2019-003) has been deposited at the College of Pharmacy, Wonkwang University, Korea.

Extraction and isolation
The dried rhizomes of *A. macrocephala* (2.0 kg) were cut and extracted using MeOH three times for 3 h at 80 °C. The resultant MeOH extract (100.9 g) was suspended in water (1.0 L × 3) and then sequentially partitioned using equal volumes of n-hexane, dichloromethane, ethyl acetate, and n-butanol. Each fraction was evaporated in vacuo to yield the residues of n-hexane (8.9 g), CH_2Cl_2 (3.7 g), EtOAc (1.5 g), n-BuOH (3.9 g), and water (72.3 g) extracts, respectively.

The n-hexane soluble fraction (8.5 g) was subjected to column chromatography (CC) using a silica gel column and eluted with an n-hexane/EtOAc (100:0 → 1:1) gradient system. The fractions were combined based on their thin layer chromatography (TLC) pattern to yield subfractions, which were designated H1–H7. Fraction H1 (3.8 g) was purified by Sephadex LH-20 CC (n-hexane, 100:0) to yield six subfractions (H11–H16). Subfraction H11 was purified by silica gel CC (n-hexane/EtOAc, 100:1 → 10:1), and by ODS CC (MeOH/H_2O, 1.5:1 → 2:1) to yield **1** (1.5 mg). In addition, subfraction H13 was purified by silica gel CC (n-hexane/EtOAc, 30:1 → 10:1), and by ODS CC (MeOH/H_2O, 1:1 → 3:1) to yield **9** (12.0 mg) and **5** (90.2 mg). Subfraction H15 was purified by silica gel CC (n-hexane/EtOAc, 20:1 → 5:1), and by ODS CC (MeOH/H_2O, 1:1 → 2:1) to yield **6** (2.6 mg). Fraction H2 (1.1 g) was subjected to silica gel CC eluting with an n-hexane/EtOAc (50:1 → 10:1) gradient system to yield three subfractions (H21–H23). Subfraction H21 was then purified by repeated ODS CC (MeOH/H_2O, 2.5:1 → 3.5:1) to yield **3** (13.2 mg), and **8** (50.6 mg). Fraction H3 (1.2 g) was subjected to silica gel CC eluting with a n-hexane/EtOAc (15:1 → 5:1) gradient system to yield six subfractions (H31–H36). Subfraction H31 was purified by silica gel CC (n-hexane/EtOAc, 25:1 → 15:1), and by ODS CC (MeOH/H_2O, 1.5:1 → 3.5:1) to yield **4** (55.6 mg) and **7** (165.6 mg). Moreover, subfraction H34 was then purified by ODS CC (MeOH/H_2O, 4.5:1 → 6:1) to yield **11** (73.2 mg), and **12** (23.0 mg). Fraction H4 (435.2 mg) was subjected to silica gel CC eluting with a n-hexane/EtOAc (8:1 → 4:1) gradient system to achieve five subfractions (H41–H45). Subfraction H42 was purified by ODS CC (MeOH/H_2O, 1.5:1 → 3:1) to yield **10** (13.2 mg).

The CH_2Cl_2 soluble fraction (3.5 g) was subjected to CC using a Sephadex LH 20 column and eluted with CH_2Cl_2/MeOH (1:1 and 100% MeOH) system. The fractions were combined based on their TLC pattern to yield subfractions, which were designated D1–D4. Fraction D2 (596.8 mg) was subjected to silica gel CC eluting with n-hexane/EtOAc (5:1 → 1:1) gradient system to yield eight subfractions (D21–D28). Subfraction D25 was purified by ODS CC (MeOH/H_2O, 1:1 → 2:1), followed by preparative high-performance liquid chromatography (HPLC) eluted with MeOH/H_2O (60:40) to give **14** (12.4 mg). Fraction D3 (464.6 g), containing **15**, and **16** was purified by silica gel CC n-hexane/EtOAc (4:1 → 1:1), followed by medium pressure liquid chromatography

Jin *et al. Applied Biological Chemistry* (2022) 65:11

Page 3 of 13

(MPLC) (MeOH/H_2O, 3:1 → 1:1), and finally by ODS CC (MeOH/H_2O, 2:1 → 1:1) to give **15** (33.2 mg) and **16** (11.2 mg).

The EtOAc soluble fraction (1.1 g) was subjected to CC using a silica gel column and eluted with $CHCl_3$/MeOH/H_2O (20:1:0.1 → 1:1:0.1) gradient system. The fractions were combined based on their TLC pattern to yield subfractions, which were designated E1–E10. Fraction E3 (135.7 mg) was subjected to ODS CC eluting with MeOH/H_2O (3:1 → 1.5:1) gradient system to give six subfractions (E31–E36). Subfraction E33 was purified by silica gel CC ($CHCl_3$/MeOH, 9:1) to give **12** (32.2 mg). Fraction E5 (359.2 mg) was subjected to silica gel CC eluting with a $CHCl_3$/MeOH/H_2O (4:1:0.1 → 1:1:0.1) gradient system to give six subfractions (E51–E56). Subfraction E53 was purified by MPLC (MeOH/H_2O, 1:4 → 1:3), and by ODS CC (MeOH/H_2O, 1:3.5) to give **17** (8.3 mg) and **18** (6.0 mg). Fraction E8 (204.5 mg) was subjected to silica gel CC eluting with $CHCl_3$/MeOH/H_2O (3:1:0.1 → 1:1:0.1) gradient system to give eight subfractions (E81-E88). Subfraction E85 was purified by ODS CC (MeOH/H_2O, 1:2 → 1:1), followed by preparative HPLC eluting with MeOH/H_2O (20:80 → 60:40) gradient system, to give **19** (10.6 mg), **20** (2.6 mg), and **21** (9.8 mg). Besides, subfraction E87 was purified by ODS CC (MeOH/H_2O, 1:1.5) to give **22** (14.5 mg).

Chemicals and reagents

Tissue culture reagents RPMI1640, Dulbecco's modified Eagle's medium (DMEM) and fetal bovine serum (FBS) were obtained from Gibco BRL Co. (Grand Island, NY, USA). LPS was purchased from Sigma-Aldrich (St. Louis, MO, USA). 3-[4,5-dimethylthiazol-2-yl]-2, 5-diphenyltetrazolium bromide sodium (MTT) was obtained from Glentham Life Sciences (Corsham, UK). The anti-inducible nitric oxide synthase (iNOS) primary antibodies were purchased from Cayman (Ann Arbor, MI, USA), anti-cyclooxygenase (COX)-2, anti-inhibitor kappa B (IκB)-a, anti-p-IκB-a, anti-p-p65, anti-p65, anti-p-extracellular signal-regulated kinase (ERK), anti-ERK, anti-p-c-Jun N-terminal kinase (JNK), anti-JNK, anti-p-p38, and anti-p38 from Cell Signaling (Danvers, MA), and anti-β-actin from Santa Cruz Biotechnology (Dallas, TX, USA), respectively. Anti-mouse, anti-goat, and anti-rabbit secondary antibodies were purchased from Merck Millipore (Darmstadt, Germany).

Cell culture

The immortalized murine RAW264.7 macrophages and BV2 microglial cells were maintained at 5×10^5 cells/mL in 100 mm dishes in RPMI1640 medium supplemented with 10% (v/v) heat-inactivated FBS, penicillin G (100 units/mL), streptomycin (100 mg/mL), and L-glutamine (2 mM), and cultured at 37 °C in a humidified atmosphere containing 5% CO_2.

Cell viability assay

An MTT assay was conducted to determine cell viability. RAW264.7 and BV2 cells were cultured in a 96-well plate at a density 1×10^5 cell/mL, and the cultured cells were treated with the test compounds for 24 h. Subsequently, 50 μL of an MTT solution were added to each well at a final concentration of 0.5 mg/mL, and the cells were incubated for 3 h in a humidified incubator at 37 °C. After removing the supernatant, the formazan formed was dissolved in 150 μL of dimethyl sulfoxide (DMSO), and mixed for 15 min. The optical density of the DMSO solution was measured at 540 nm wavelength using a microplate reader (Bio-Rad, Hercules, CA, USA). The optical density of the formazan formed in the control (untreated group) cells was considered to represent 100% viability, and the viability of cells in other groups was expressed as a percentage of obtained viable cells relative to the control. This assay was independently conducted three times.

Determination of nitrite

Nitrite is an indicator of NO production; its concentration in the culture medium was measured using the Griess reaction. RAW264.7 and BV2 cells were cultured in a 24-well plate at a density of 2×10^5 cell/mL for 12 h. Cells were treated with test compounds for 3 h, and then stimulated with LPS (1 μg/mL) for 24 h. Each culture medium (100 μL) was mixed with the same volume of Griess reagent (Sigma-Aldrich, St. Louis, MO, USA) for 15 min at room temperature. The absorbance was measured spectrophotometrically at 540 nm wavelength using an enzyme-linked immunosorbent assay (ELISA) plate reader. The nitrite concentration in the culture medium was determined from a standard curve of sodium nitrite.

PGE_2 assay

The culture media were collected to determine the PGE_2 level present in each sample using the appropriate ELISA kit from ENZO Life Sciences (Farmingdale, NY, USA). Three independent assays were performed according to the manufacturer's instructions.

IL-1β, IL-6, and TNF-α assays

The levels of IL-1β, IL-6, and TNF-α present in each sample were determined using a commercially appropriate kit from R&D Systems (Minneapolis, MN). Three independent assays were performed according to the manufacturer's instructions.

Jin *et al. Applied Biological Chemistry*   (2022) 65:11

Page 4 of 13

Western blot analysis

RAW264.7 and BV2 cells were cultured in a 6-well plate at a density of 2×10^5 cell/mL for 12 h. Then cells were treated with the test compounds for 3 h, followed by stimulation with LPS (1 μg/mL) for 24 h. Radioimmunoprecipitation assay (RIPA) buffer (Thermo Scientific, MA, USA) was used to prepare lysate. The concentration of protein was measured using Bradford protein assay (Bio-Rad Laboratories, CA, USA) and normalized to ensure that equal amounts were loaded. Subsequently, 30 μg of protein from each sample were resolved using 6%, 8%, and 12% sodium dodecyl sulfate–polyacrylamide gel electrophoresis (SDS–PAGE). The proteins were electrophoretically transferred onto Hybond enhanced chemiluminescence (ECL) nitrocellulose membranes (Bio-Rad, Hercules, CA, USA). The membranes were blocked with 5% skim milk and sequentially incubated with particular primary antibodies and horseradish peroxidase (HRP)-conjugated secondary antibodies, followed by ECL detection (Amersham Pharmacia Biotech, Piscataway, NJ, USA).
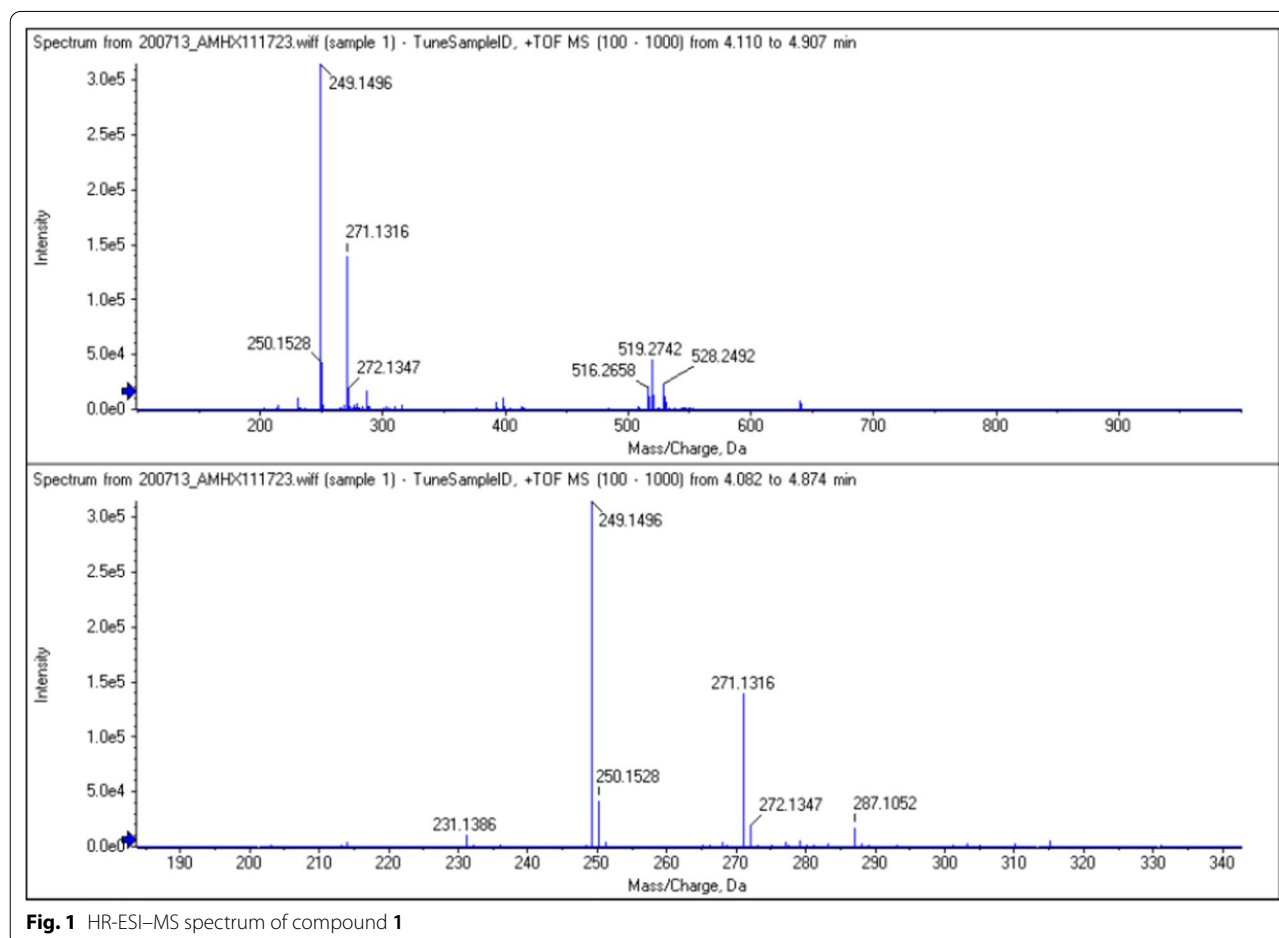
Statistical analysis

The data are expressed as mean ± standard deviation (SD) of at least three independent experiments. To compare three or more groups, a one-way analysis of variance (ANOVA) was used, followed by Tukey's multiple comparison tests. Statistical analysis was performed using GraphPad Prism software, version 3.03 (GraphPad Software Inc., San Diego, CA, USA).

Results

Compounds isolated from *A. macrocephala*

Twenty-two compounds were isolated from the rhizomes of *A. macrocephala* using various combined chromatographic methods. The nuclear magnetic resonance (NMR) and mass spectroscopy (MS) data of the isolated compounds were analyzed and compared with those reported in the literature to elucidate the structures of the isolated compounds. Compound **1** was obtained as a white solid. $[\alpha]_D^{23} + 232.4$ (c 0.07, MeOH). Its molecular formula of $C_{15}H_{20}O_3$ was determined based on the analysis of HR-ESI-MS data showing m/z peak at 249.1496 $[M+H]^+$ (calculated for $C_{15}H_{21}O_3$: 249.1412) (Fig. 1),

Fig. 1 HR-ESI–MS spectrum of compound **1**

Jin *et al. Applied Biological Chemistry*   (2022) 65:11

Page 5 of 13

and the analysis of ^{1}H NMR and ^{13}C NMR data (Table 1, Fig. 2, Additional file 1: Fig. S1). The ^{1}H-NMR spectrum of **1** (in CDCl$_3$) showed the following signals: two tertiary methyl groups at δ 0.89 (3H, s) and 1.83 (3H, t, J = 1.6 Hz), which were typical of CH$_3$-14 and CH$_3$-13 of eudesmanolides; together with one terminal double bond at δ 4.60 (1H, d, J = 1.6 Hz) and 4.88 (1H, d, J = 1.6 Hz) for H-15. The ^{1}H-NMR patterns of **1** were similar to those of the known compound **5** (atractylenolide II) [21], as stated in the Supplementary data. However, the ^{1}H-NMR spectrum of **1** was distinct from that of **5** because there was one more proton signal at δ 3.88 (1H, d, J = 3.6 Hz). Moreover, in ^{13}C-NMR spectrum, there was an additional carbon signal at δ 75.4. Taking the molecular formula into account, it was suggested that hydroxylation

had taken place on one of the secondary carbons. Compared with **5**, H-8 signals of **1** notably shifted to lower fields, from δ 4.80 (1H, t, J = 6.4 Hz) to δ 4.98 (1H, d, J = 2.0 Hz). Therefore, it was supposed that a hydroxylation took place at C-9, resulting in increased chemical shift values of H-8 for an inductive effect. In the heteronuclear multiple bond correlation (HMBC) spectrum, the long-range correlations from the carbon signal at δ 75.4 (C-9), to H-8 signals confirmed the hydroxyl group located at C-9 (Table 1, Additional file 1: Fig. S3, S5). The coupling constants and the cross peak between H-9 and the signal at δ 4.98 (1H, d, J = 2.0 Hz) and δ 0.89 (3H, s), assigned to H-8 and CH$_3$-14, respectively, also CH$_3$-14 correlated with H-2β, in NOESY spectrum confirmed that the H-9 was axial and β-oriented (Additional file 1: Fig. S4, S6). Finally, the chemical structure of **1** is formed by adding an extra oxygen in comparison with **5**, and **1** was established as 9α-hydroxyatractylenolide, namely 9α-hydroxyeudesma-4(15),7(11)-dien-8α,12-olide. When compound **1** was separated and purified by ODS CC, it was found that its R$_f$ value was very close to that of compound **7** by TLC analysis. It was worth noting that **1** has no fluorescence under 254 nm ultraviolet light, while **7** shows dark brown fluorescence. After heating and color development spraying with 10% sulfuric acid, **1** showed blue-purple and blue fluorescence, however, **7** showed dark brown and yellow-green fluorescence at 254 and 365 nm, respectively. There was a significant difference between the two compounds. This difference is related to the position of OH. The lone pair electron on the 8-position OH of **7** formed a p-π conjugation effect with a double bond and carbonyl, enhancing the fluorescence, while the OH in **1** did not have the above effect at the 9-position. As far as we know, its spectroscopic data had not been reported before. In addition, the other compounds were identified by comparing with previously published data as presented in Fig. 3.

Table 1 NMR data for compound **1** in CDCl$_3$

No	δC^a	δH (J, Hz)^b	HMBC
1	34.6	1.33 (1H, m)	C_2, C_{10}, C_{14}
		2.06 (1H, dd, J = 13.6, 4.4 Hz)	
2	22.3	1.60 (2H, m)	
3	36.3	1.96 (1H, m)	C_2, C_4, C_{15}
		2.35 (1H, m)	C_4
4	148.9		
5	42.2	2.38 (1H, m)	C_{10}
6	25.6	2.31 (1H, m)	C_7, C_{10}
		2.67 (1H, dq, J = 12.8, 2.8 Hz)	C_7, C_8, C_{10}
7	159.1		
8	79.9	4.98 (1H, d, J = 2.0 Hz)	
9	75.4	3.88 (1H, d, J = 3.6 Hz)	C_5, C_7, C_8
10	41.0		
11	121.9		
12	175.1		
13	8.4	1.83 (3H, t, J = 1.6 Hz)	C_7, C_{11}, C_{12}
14	15.7	0.89 (3H, s)	C_1, C_5, C_9, C_{10}
15	107.3	4.88 (1H, d, J = 1.6 Hz)	C_3, C_5
		4.60 (1H, d, J = 1.6 Hz)	

Fig. 2 The key HMBC (**A**) and NOESY (**B**) correlations (arrow) of compound **1**

Jin *et al. Applied Biological Chemistry*   (2022) 65:11

Page 6 of 13

Fig. 3 The chemical structures of compounds **1**–**22** isolated from *Atractylodes macrocephala*
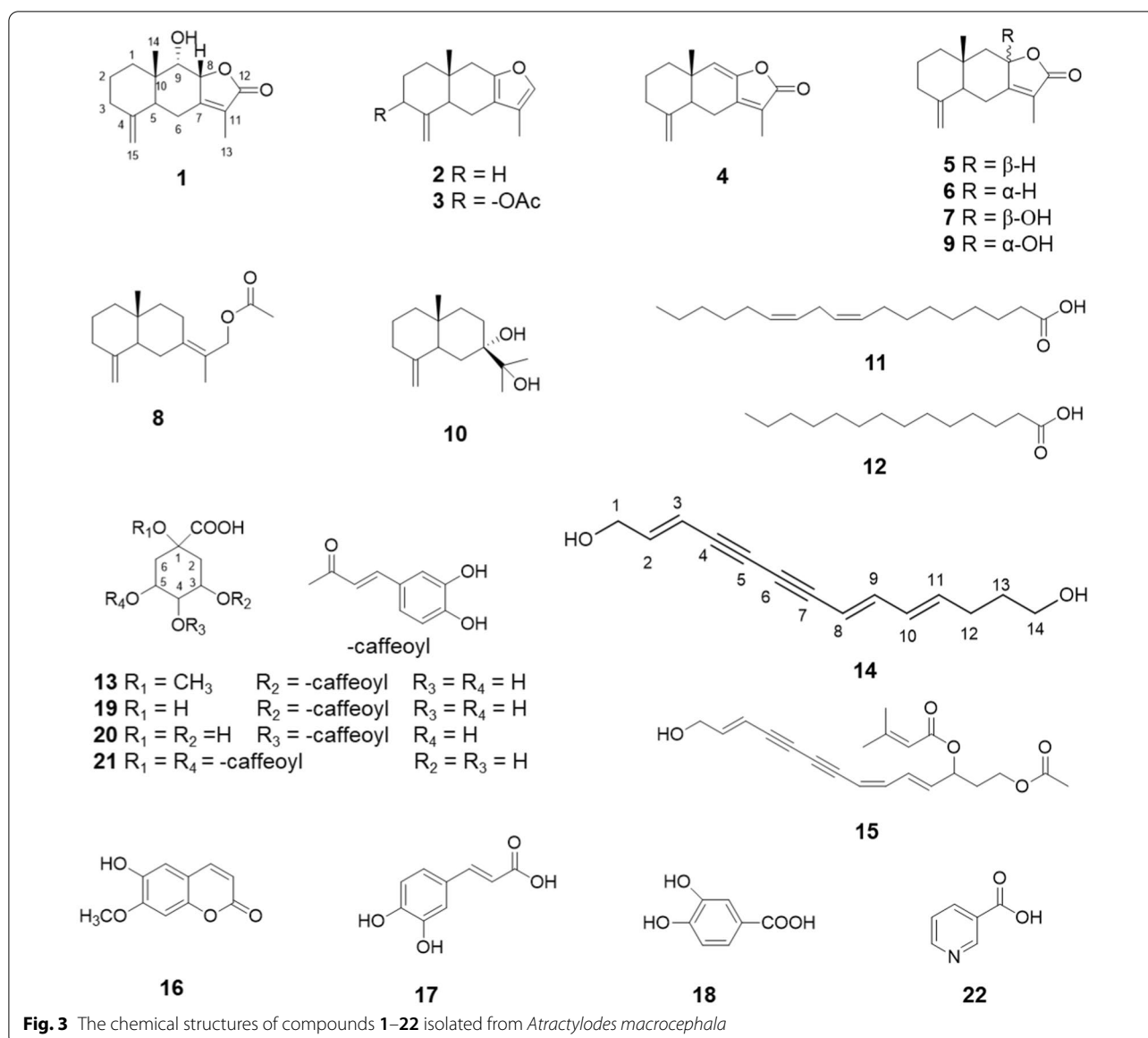
Comparing with previously published data, the other compounds were identified as atractylone (**2**) [22], 3β-acetoxyatractylon (**3**) [22], atractylenolide I (**4**) [23], atractylenolide II (**5**) [21], 8-epiasterolid (**6**) [24], atractylenolide III (**7**) [14], atractylenolide VII (**8**) [25], 8-epiatractylenolide III (**9**) [14], eudesm-4(15)-ene-7α,11-diol (**10**) [26], linoleic acid (**11**) [27], myristic acid (**12**) [27], 3-*O*-caffeoyl-1-methyquinic acid (**13**) [28], (2*E*,8*E*,10*E*)-tetradecatriene-4,6-diyne-1,14-diol (**14**) [29],

14-aceroxy-12-senecioyloxytetradeca-2*E*,8*Z*,10*E*-trien-4,6-diyn-1-ol (**15**) [30], isoscopoletin (**16**) [31], caffeic acid (**17**) [32], protocatechic acid (**18**) [33], 3-*O*-caffeoylquinic acid (**19**) [28], 4-*O*-caffeoylquinic acid (**20**) [34], 1,5-di-*O*-caffeoylquinic acid (**21**) [35], and nicotinic acid (**22**) [36] (Fig. 3).

Although we tried to evaluate the bioactivity of the isolated compounds, the amounts of compounds **1**, **3** and **20** were too small to determine their bioactivities. In addition, compound **2** was obtained in a sufficient amount, but further NMR analysis indicated changes in the compound. Thus, the remaining 18 compounds were used to examine their bioactivity.

Inhibitory effect of compounds isolated from *A. macrocephala* on LPS-induced NO production in RAW264.7 and BV2 cells

First, we evaluated whether the compounds exerted a cytotoxic effect on RAW264.7 and BV2 cells. Cells were treated with 5, 10, 20, 40, and 80 μM of selected compounds for 24 h, and cell viability was measured
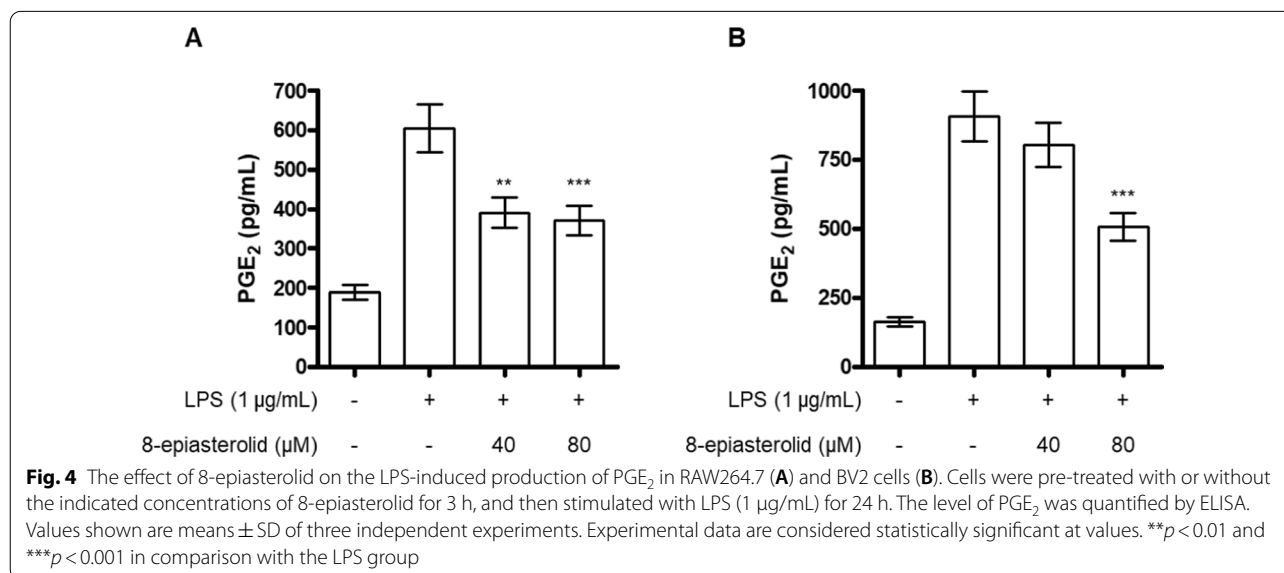
Table 2 Inhibitory effects of the test compounds on LPS-induced NO production in RAW264.7 and BV2 cells

Compounds	IC_{50} (μM)	
	RAW264.7	**BV2**
Butein	5.40 ± 0.50	4.41 ± 0.45
4	26.8 ± 3.86	26.0 ± 0.23
5	60.5 ± 16.8	46.8 ± 1.12
6	39.1 ± 3.22	37.4 ± 4.03
7	1.7% at 80 μM	20.3% at 80 μM
8	50.8 ± 7.38	35.9% at 80 μM
9	9.2% at 80 μM	27.3% at 80 μM
10	64.3 ± 12.1	24.2% at 80 μM
11	41.2 ± 4.97	47.7% at 80 μM
12	36.7 ± 4.11	35.9% at 80 μM
13	59.2 ± 14.9	25.0% at 80 μM
14	28.4 ± 6.55	29.7% at 80 μM
15	51.3 ± 7.28	38.9% at 80 μM
16	29.8 ± 2.52	58.5 ± 2.23
17	34.8 ± 2.54	72.3 ± 3.35
18	44.5 ± 4.34	41.7% at 80 μM
19	28.8 ± 3.09	45.8% at 80 μM
21	78.1 ± 23.5	36.7% at 80 μM
22	28.0 ± 2.94	47.2% at 80 μM

by MTT assay. The compounds showed no cytotoxicity for any of the tested concentrations (data not shown). Therefore, the three highest concentrations (20, 40, and 80 μM) were used in the NO assay. Cells were pre-treated with 20, 40, and 80 μM of compounds for 3 h, and then stimulated with LPS (1 μg/mL) for 24 h. Regarding RAW264.7 cells, most compounds inhibited the LPS-induced NO production, except for compounds **7** and **9**, with IC_{50} values in the 26.8–78.1 μM range. In BV2 cells, all the tested compounds suppressed NO production in a concentration-dependent manner. Compounds **4**, **5**, **6**, **16**, and **17**, showed an inhibitory effect higher than 50% within the used concentration range, with IC_{50} values of 26.0 ± 0.23, 46.8 ± 1.12, 37.4 ± 4.03, 58.5 ± 2.23, and 72.3 ± 3.35 μM, respectively (Table 2).

Inhibitory effect of 8-epiasterolid on LPS-induced PGE_2 production in RAW264.7 and BV2 cells

According to the above result, atractylenolide I (**4**) showed the lowest IC_{50} value in both RAW264.7 and BV2 cells. However, the anti-inflammatory and anti-neuroinflammatory effects of this compound was already reported [16, 17]. Therefore, we selected 8-epiasterolid (**6**), which was the second most effective, and examined its further anti-inflammatory activity. RAW264.7 and BV2 cells were pre-treated with 8-epiasterolid for 3 h, followed by stimulation with LPS (1 μg/mL) for 24 h to examine whether it affected PGE_2 production. It was found that pre-treatment with 8-epiasterolid significantly inhibited the LPS-induced PGE_2 production in both RAW264.7 and BV2 cells (Fig. 4).

Fig. 4 The effect of 8-epiasterolid on the LPS-induced production of PGE_2 in RAW264.7 (**A**) and BV2 cells (**B**). Cells were pre-treated with or without the indicated concentrations of 8-epiasterolid for 3 h, and then stimulated with LPS (1 μg/mL) for 24 h. The level of PGE_2 was quantified by ELISA. Values shown are means ± SD of three independent experiments. Experimental data are considered statistically significant at values. **$p < 0.01$ and ***$p < 0.001$ in comparison with the LPS group

Jin *et al. Applied Biological Chemistry*   (2022) 65:11

Page 8 of 13

Inhibitory effect of 8-epiasterolid on LPS-induced production of pro-inflammatory cytokines in RAW264.7 and BV2 cells

Based on the above results, we examined whether 8-epiasterolid suppressed the production of pro-inflammatory cytokines in LPS-induced RAW264.7 and BV2 cells. Both cells were pre-treated with 8-epiasterolid for 3 h, and then stimulated with LPS (1 µg/mL) for 24 h. At a concentration of 80 µM, 8-epiasterolid significantly suppressed the LPS-induced production of IL-1β, IL-6, and TNF-α in both RAW264.7 and BV2 cells (Fig. 5).

Inhibitory effect of 8-epiasterolid on LPS-induced iNOS and COX-2 expression in RAW264.7 and BV2 cells

We further investigated the effect of 8-epiasterolid on the expression of iNOS and COX-2 proteins induced by LPS in both cell lines. Cells were pre-treated with 8-epiasterolid for 3 h, and then stimulated with LPS (1 µg/mL) for 24 h. The degree of expression of iNOS and COX-2 proteins in the lysates was determined using Western blot analysis. The pre-treatment with 8-epiasterolid at concentrations of 40 and 80 µM suppressed the LPS-induced iNOS and COX-2 expression in both RAW264.7 and BV2 cells (Fig. 6).
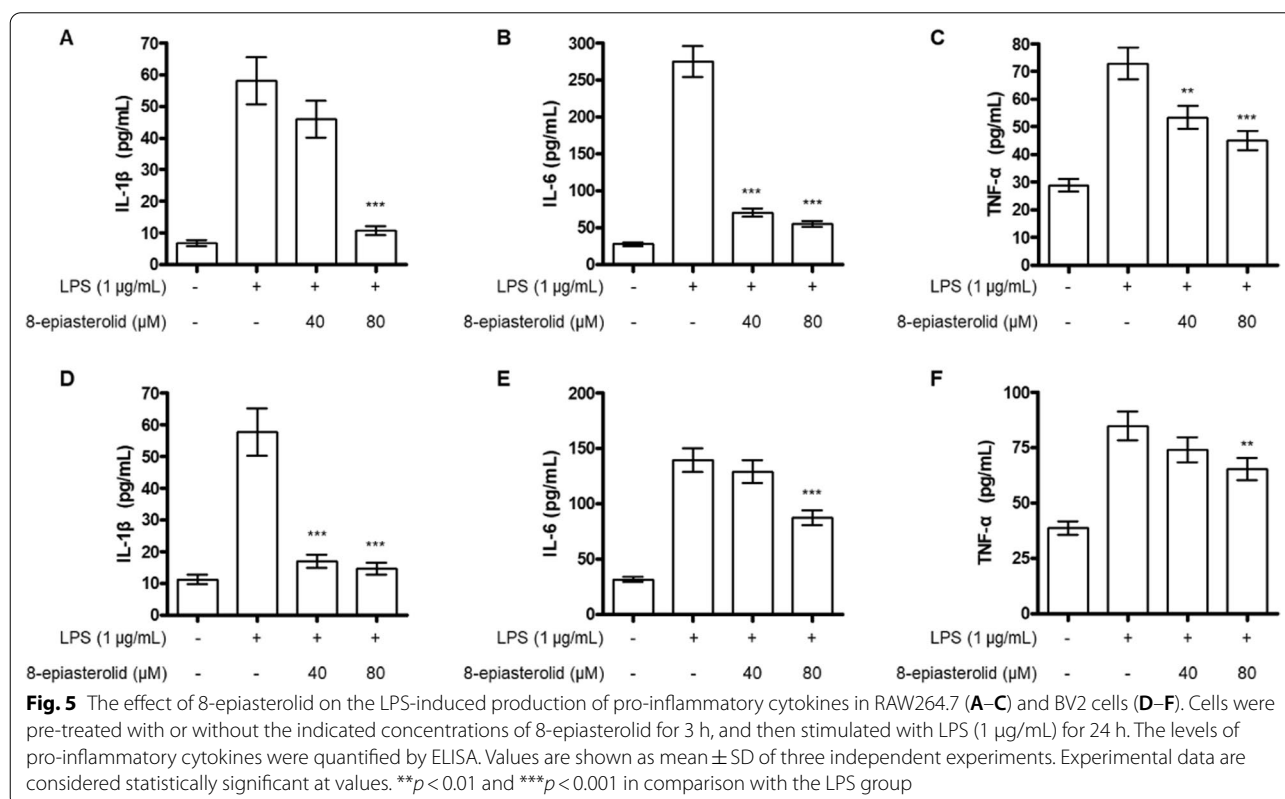
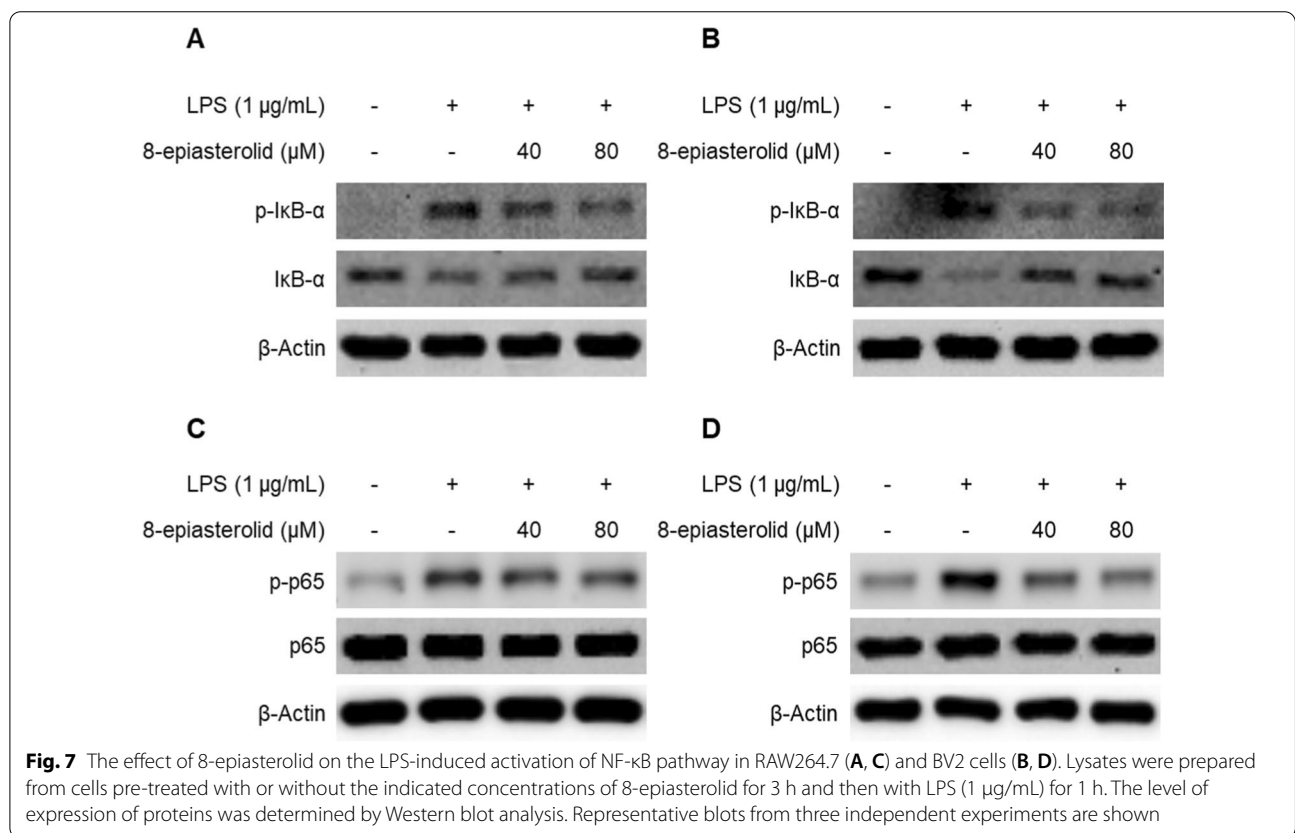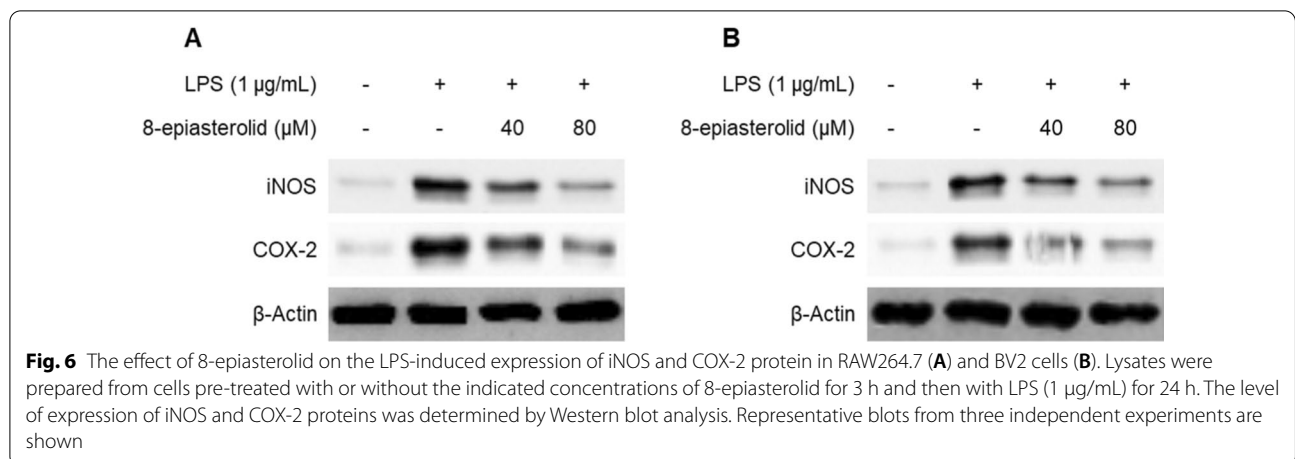### Effect of 8-epiasterolid on the LPS-induced activation of NF-κB and MAPK signaling pathways

We examined whether 8-epiasterolid suppressed the activation of NF-κB pathway in LPS-induced RAW264.7 and BV2 cells. Both cell lines were pre-treated with 8-epiasterolid for 3 h, and then stimulated with LPS (1 µg/mL) for 1 h. The pre-treatment with 8-epiasterolid inhibited the LPS-induced phosphorylation and degradation of IκB-α as well as the phosphorylation of p65 in both RAW264.7 and BV2 cells (Fig. 7).

Additionally, we investigated whether 8-epiasterolid affects the LPS-induced activation of the MAPK pathways in RAW264.7 and BV2 cells. Both cell lines were pre-treated with 8-epiasterolid for 3 h, and then stimulated with LPS (1 µg/mL) for 30 min. The phosphorylation levels of p38, ERK, and JNK remarkably increased by LPS-stimulation. However, the pre-treatment with 8-epiasterolid did not inhibit the activation of all three MAPKs (Fig. 8).
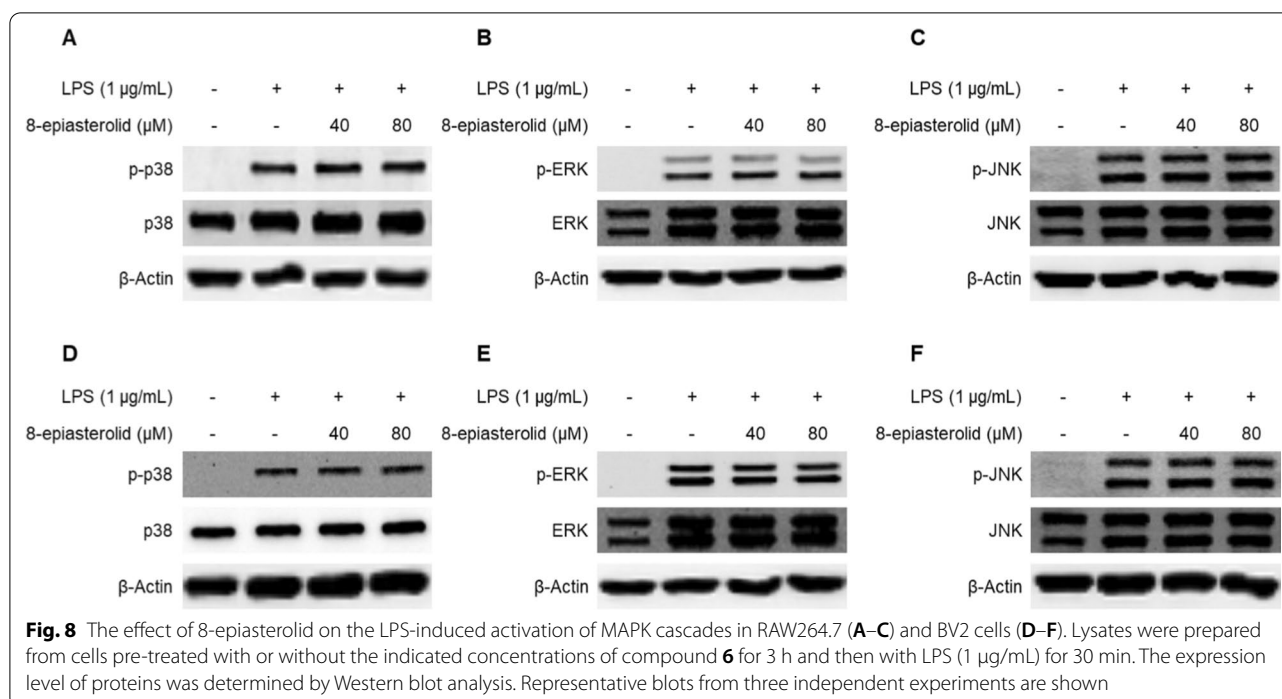
Discussion

In this investigation, we isolated 22 compounds from the rhizomes of *A. macrocephala* using various combined chromatographic methods, and evaluated their anti-inflammatory effects measuring the degree of the production of NO in LPS-induced RAW264.7 and

Fig. 5 The effect of 8-epiasterolid on the LPS-induced production of pro-inflammatory cytokines in RAW264.7 (**A**–**C**) and BV2 cells (**D**–**F**). Cells were pre-treated with or without the indicated concentrations of 8-epiasterolid for 3 h, and then stimulated with LPS (1 µg/mL) for 24 h. The levels of pro-inflammatory cytokines were quantified by ELISA. Values are shown as mean ± SD of three independent experiments. Experimental data are considered statistically significant at values. **$p < 0.01$ and ***$p < 0.001$ in comparison with the LPS group

Fig. 6 The effect of 8-epiasterolid on the LPS-induced expression of iNOS and COX-2 protein in RAW264.7 (**A**) and BV2 cells (**B**). Lysates were prepared from cells pre-treated with or without the indicated concentrations of 8-epiasterolid for 3 h and then with LPS (1 μg/mL) for 24 h. The level of expression of iNOS and COX-2 proteins was determined by Western blot analysis. Representative blots from three independent experiments are shown

Fig. 7 The effect of 8-epiasterolid on the LPS-induced activation of NF-κB pathway in RAW264.7 (**A**, **C**) and BV2 cells (**B**, **D**). Lysates were prepared from cells pre-treated with or without the indicated concentrations of 8-epiasterolid for 3 h and then with LPS (1 μg/mL) for 1 h. The level of expression of proteins was determined by Western blot analysis. Representative blots from three independent experiments are shown

BV2 cells. Among them, we found that 8-epiasterolid is the second most effect compound, and it inhibited the LPS-induced production of PGE$_2$ and pro-inflammatory cytokines, and the expression of iNOS and COX-2 proteins. In addition, we confirmed that these inhibitory effects were regulated by the inactivation of NF-κB signaling pathway by 8-epiasterolid, not MAPK pathways.

The production of NO is catalyzed by the enzymatic activity of nitric oxide synthase (NOS), which converts L-arginine to NO and L-citrulline via the intermediate N-hydroxy-L-arginine [37, 38]. NO is known to play a key role in regulating the vascular, immune, and nervous systems [39]. In inflammatory conditions, the expression of NOS increases in various immune cells including macrophages, monocytes, microglia, dendritic cells,

Jin *et al. Applied Biological Chemistry* (2022) 65:11

Page 10 of 13

Fig. 8 The effect of 8-epiasterolid on the LPS-induced activation of MAPK cascades in RAW264.7 (**A**–**C**) and BV2 cells (**D**–**F**). Lysates were prepared from cells pre-treated with or without the indicated concentrations of compound **6** for 3 h and then with LPS (1 μg/mL) for 30 min. The expression level of proteins was determined by Western blot analysis. Representative blots from three independent experiments are shown

eosinophils, and neutrophils, resulting in the release of large amounts of NO [38]. Subsequently, the overproduction of NO leads to development of inflammatory disorders in the joints, gut, and lungs [38], neurodegenerative diseases including Alzheimer's disease, Parkinson's disease, multiple sclerosis [39], and cancer [40]. As inhibiting NO production could have a therapeutic effect on inflammatory diseases, we investigated whether the compounds isolated from *A. macrocephala* might inhibit the LPS-induced NO production in RAW264.7 macrophages and BV2 microglial cells. Our result showed that atractylenolide I (compound **4**) has the lowest IC$_{50}$ value among the tested compounds, indicating that it has the highest inhibitory effect. Previous studies have reported that atractylenolide I has anti-inflammatory effects in RAW264.7 macrophages by inhibiting the activation of NF-κB and MAPK signaling pathways mediated through the cluster of differentiation 14 (CD14)/toll-like receptor 4 (TLR4) pathways [16]. This compound also showed neuroprotective effects through the suppression of NF-κB pathway and induction of heme oxygenase (HO)-1 protein in BV2 microglia cells and in 1-methyl-4-phenyl-1,2,3,6-tetrahydropyridine (MPTP)-induced C57BL6/J models, suggesting that atractylenolide I might be effective in treating Parkinson's disease [17]. 8-Epiasterolid was the second most effective compound for NO production in both RAW264.7 and BV2 cells; additional experiments were conducted and showed that this compound possesses anti-inflammatory properties (Table 2).

As mentioned in "Introduction" section, macrophages are the most dominant immune cell types throughout the body, and microglia play as the first and main form of active immune defense in CNS as the resident macrophage cells in nerve system. Both cells exhibit the characteristics of macrophages, but microglial cells are specialized ones that are only found in the nerve system (brain and spinal cord) [41]. In addition, Luigina Guasti et al. investigated the in vitro effects of Apixaban (commercial product named Eliquis®) on cell proliferation, mortality, cell migration, gene expression and matrix metalloproteinase (MMP) in 5 different cancer cell lines including OVCAR3 (ovarian cancer), MDA MB 231 (breast cancer), CaCO-2 (colon cancer), LNCaP (prostate cancer), and U937 (histiocytic lymphoma). They reported that Apixaban increased the expression of tumor suppression gene p16 in all cell lines, but reduced proliferation in only 3 cancer cell lines (OVCAR3, CaCO-2, and LNCaP) [42]. These results suggest that the same compound might exhibit different effects in different cell lines. Therefore, the effects of tested compound isolated from *A. macrocephala* applied to different cells (RAW264.7 macrophages and BV2 microglial cells) could be different.

Similar to NO, prostaglandins play an important role in the inflammatory process. Arachidonic acid (AA) in the body is converted into prostaglandin H2 (PGH$_2$) by the action of cyclooxygenase (COX)-1 and 2 enzymes [43]. Then, PGH$_2$ acts as a substrate of specific isomerase

and synthase enzymes to produce various prostanoids including PGE_2, PGI_2, PGD_2, $PGF_{2\alpha}$, and thromboxane A2 (TXA_2) [44]. PGE_2 reacts with four types of receptors (EP1–EP4), each with its distinct signal-transduction properties, and exerts diverse physiological functions [45]. Our results showed that the pre-treatment with 8-epiasterolid significantly inhibited the LPS-induced production of PGE_2 in both RAW264.7 and BV2 cells (Fig. 4).

Cytokines are small secreted proteins produced by every cell and regulate the immune responses [46]. They consist of six major families including ILs, chemokines, interferons, TNF, growth factors of hematopoiesis and transforming growth factor-β (TGF-β) members [47]. In particular, the pro-inflammatory cytokines including IL-1β, IL-6 and TNF-α are produced from activated macrophages or microglia, and are associated with the up-regulation of inflammatory responses [46]. Compound **4** (atractylenolide I), which is one of the isolated compounds, has been reported that this compound inhibited the production of TNF-α and IL-6 in LPS-stimulated RAW264.7 cell model [16]. Another investigation demonstrated that compound **4** inhibited the production of TNF-α, IL-6, and IL-1β in LPS-induced BV2 microglial cell model, and that of TNF-α in MPTP-induced mice model [17]. Accordingly, we investigated the inhibitory effect of 8-epiasterolid on the LPS-induced production of pro-inflammatory cytokines in RAW264.7 and BV2 cells. Our results showed that the pre-treatment with 8-epiatsterolid markedly suppressed the production of IL-1β, IL-6, and TNF-α in both cells (Fig. 5).

NO is synthesized from the L-arginine via the enzymatic activity of NOS. There are three different isoforms of NOS including neuronal nNOS (NOS1), inducible iNOS (NOS2), and endothelial eNOS (NOS3) [48]. Each enzyme has its own physiological characteristics. nNOS is expressed in neurons, and has been reported to mediate the long-term regulation of synaptic transmission [49]. eNOS is released mainly by endothelial cells; as it promotes blood vessel expansion and controls blood pressure, the functional anomalies in eNOS lead to the development of cardiovascular diseases [49]. eNOS is also known to control cancer-related phenomena such as angiogenesis, apoptosis, invasion, and metastasis [50]. nNOS and eNOS are constitutive forms that continuously secrete low concentrations of NO, and thus maintain several physiological functions. However, since iNOS is inducible, its production is increased by bacterial LPS, cytokines, chemokines, and other stimuli such as stress [49, 51].

As mentioned above, COX is involved in the generation of PGE_2. There are two COX isoforms: COX-1 and COX-2. The former is a constitutive type that is expressed in

most tissues and is associated with conducting normal physiological functions [52, 53]. On the other hand, COX-2 is an inducible form and is up-regulated through various inflammatory stimuli of cytokines, growth factors, tumor promotors, and bacterial LPS, which then increase the amount of PGE_2 produced [54]. Although both COX-1 and COX-2 are related to the production of PGE_2, the continuous suppression of COX-1 activity could lead to side effects such as gastrointestinal toxicity or mild bleeding diathesis [55]. Therefore, the selective inhibition of COX-2 is necessary to block inflammatory responses. In previous results, 8-epiasterolid inhibited the production of NO and PGE_2 induced by LPS. Accordingly, the pre-treatment with 8-epiasterolid also repressed the LPS-induced expression of iNOS and COX-2, which are enzymatic proteins associated with the production of NO and PGE_2, respectively, in both RAW264.7 and BV2 cells (Fig. 6).

NF-κB is one of the main transcription factors that regulates gene expression and that is involved in the production of pro-inflammatory mediators [56], development of immune cells, cell cycle, proliferation, and cell death [57]. This family consists of five structurally related members, including RelA (p65), p50, p52, RelB, and c-Rel, and these subunits form at least 12 different homo- or heterodimers [58]. There are two different signaling pathways: canonical and non-canonical pathways. The canonical pathway mainly regulates RelA (p65), p50, and c-Rel, and the non-canonical pathway predominantly activates p52 and RelB. Both pathways are important for regulating immune and inflammatory responses [56, 59]. Under basal conditions, NF-κB dimers are present in the cytoplasm with their inhibitory protein IκB. However, pro-inflammatory cytokines or LPS can induce the phosphorylation and degradation of IκB, releasing NF-κB dimers and inducing phosphorylation [60]. Then, NF-κB dimers translocate into the nucleus, bind to the κB binding site, and regulate the expression of inflammatory genes including inflammatory enzymes (iNOS, COX-2), cytokines, and adhesion molecules [61]. Previous studies demonstrated that compound **4** (atractylenolide I) inhibited the LPS-induced activation of NF-κB in RAW264.7 and BV2 cells [16, 17]. Our investigation revealed that the pre-treatment with 8-epiasterolid inhibited the phosphorylation and degradation of IκB-α, and the phosphorylation of p65 protein in both RAW264.7 and BV2 cells (Fig. 7).

MAPK cascades are groups of serine/threonine protein kinases and have an important role in the transduction of extracellular signals to various cellular responses including proliferation, stress responses, apoptosis, and immune defense [62]. In mammalian cells, MAPK cascades consist of three major types, including p38, ERK,

Jin *et al. Applied Biological Chemistry*   (2022) 65:11

Page 12 of 13

and JNK MAPKs, and each kinase can be activated by many different upstream MAPK kinases (MAP2K), and MAPK kinase kinases (MAP3Ks) [63]. The phosphorylation of MAPKs has been shown to be related to the enhancement of inflammatory responses through the induction of the release of pro-inflammatory mediators [62, 64]. In a previous study, compound **4** (atractylenolide I) inhibited the LPS-induced phosphorylation of p38 and ERK MAPKs, and showed anti-inflammatory activity in RAW264.7 cells [16]. Interestingly, the pre-treatment with 8-epiasterolid did not affect to the phosphorylation of p38, ERK, and JNK MAPKs. These data suggested that 8-epiasterolid regulated the inflammatory responses by inhibiting of the NF-κB signaling pathway, not MAPK pathways.

Abbreviations

AA: Arachidonic acid; ANOVA: Analysis of variance; CC: Column chromatography; CD14: Cluster of differentiation 14 (CD14); COX-2: Cyclooxygenase-2; DMEM: Dulbecco's modified Eagle's medium; DMSO: Dimethyl sulfoxide; ECL: Enhanced chemiluminescence; ELISA: Enzyme-linked immunosorbent assay; FBS: Fetal bovine serum; HO-1: Heme oxygenase-1; HRP: Horseradish peroxidase; IL: Interleukin; iNOS: Inducible nitric oxide synthase; LPS: Lipopolysaccharide; MAPK: Mitogen-activated protein kinase; MPTP: 1-Methyl-4-phenyl-1,2,3,6-tetrahydropyridine (MPTP); MS: Mass spectroscopy; MTT: 3-[4,5-Dimethylthiazol-2-yl]-2, 5-diphenyltetrazolium bromide sodium; NF-κB: Nuclear factor kappa-light-chain-enhancer of activated B cells; NMR: Nuclear magnetic resonance; NO: Nitric oxide; NOS: Nitric oxide synthase; Nrf2: Nuclear factor erythroid 2-related factor 2; PGE_2: Prostaglandin E2; PGH_2: Prostaglandin H2; RIPA: Radioimmunoprecipitation assay; SD: Standard deviation; SDS–PAGE: Sodium dodecyl sulfate–polyacrylamide gel electrophoresis; TLC: Thin layer chromatography; TLR4: Toll-like receptor 4; TNF: Tumor necrosis factor.

Supplementary Information

The online version contains supplementary material available at https://doi.org/10.1186/s13765-022-00673-2.

Additional file 1: Figure S1. ^{1}H-NMR spectrum of compound **1** in $CDCl_3$. Figure S2. ^{13}C-NMR spectrum of compound **1** in $CDCl_3$. Figure S3. HMBC spectrum of compound **1** in $CDCl_3$. Figure S4. NOESY spectrum of compound **1** in $CDCl_3$. Figure S5. The key HMBC correlation of compound **1**. Figure S6. The key NOESY correlation of compound **1**.

Authors' contributions

All authors contributed to the study conception and design. Dae Young Lee, Dahye Yoon, Jin Tae Jeong, and Geum-Soog Kim prepared the plant materials and funded for this investigation. Youn-Chul Kim, Ren-Bo An, and Hyuncheol Oh managed the research project, provided guidance and supervised the study. Hong-Guang Jin and Ren-Bo An contributed to the isolation of compounds, and the conduction of HPLC and NMR. Kwan-Woo Kim and Jing Li carried out the biological assays. The first draft of the manuscript was written by Hong-Guang Jin and Kwan-Woo Kim. All authors read and approved the final manuscript.

Availability of data and materials

The datasets generated and analyzed during the current study are available from the corresponding author on reasonable request.

Declarations

Competing interests

The authors declare that they have no competing interests.

Author details

[1]Institute of Pharmaceutical Research and Development, College of Pharmacy, Wonkwang University, Iksan 54538, Republic of Korea. [2]School of Pharmacy and Life Sciences, Jiujiang University, Jiujiang 332005, Jiangxi, China. [3]Department of Pharmacy, Jiujiang University Hospital, Jiujiang 332000, Jiangxi, China. [4]Department of Herbal Crop Research, National Institute of Horticultural and Herbal Science, RDA, Eumseong 27709, Republic of Korea. [5]College of Pharmacy, Yanbian University, Yanji 133002, Jilin, People's Republic of China.

References

1. Abarikwu SO (2014) Kolaviron, a natural flavonoid from the seeds of *Garcinia kola*, reduces LPS-induced inflammation in macrophages by combined inhibition of IL-6 secretion, and inflammatory transcription factors, ERK1/2, NF-κB, p38, Akt, p-c-JUN and JNK. Biochim Biophys Acta 1840(7):2373–2381
2. Bain CC, Mowar AM (2014) Macrophages in intestinal homeostasis and inflammation. Immunol Rev 260(1):102–117
3. Liu YC, Zou XB, Chai YF, Yao YM (2014) Macrophage polarization in inflammatory diseases. Int J Biol Sci 10(5):520–9
4. Navarro V, Sanchez-Mejias E, Jimenez S, Muñoz-Castro C, Sanchez-Varo R, Davila JC, Vizuete M, Gutierrez A, Vitorica J (2018) Microglia in Alzheimer's disease: activated, dysfunctional or degenerative. Front Aging Neurosci. https://doi.org/10.3389/fnagi.2018.00140
5. Joe EH, Choi DJ, An J, Eun JH, Jou I, Park S (2018) Astrocytes, microglia, and Parkinson's disease. Exp Neurobiol 27(2):77–87
6. Inoue K (2006) The function of microglia through purinergic receptors: neuropathic pain and cytokine release. Pharmacol Ther 109(1–2):210–26
7. Zhang X, Li N, Shao H, Meng Y, Wang L, Wu Q, Yao Y, Li J, Bian J, Zhang Y, Deng X (2016) Methane limit LPS-induced NF-κB/MAPKs signal in macrophages and suppress immune response in mice by enhancing PI3K/AKT/GSK-3β-mediated IL-10 expression. Sci Rep. https://doi.org/10.1038/srep29359
8. Subedi L, Lee JH, Yumnam S, Ji E, Kim SY (2019) Anti-inflammatory effect of sulforaphane on LPS-activated microglia potentially through JNK/AP-1/NF-κB inhibition and Nrf2/HO-1 activation. Cells. https://doi.org/10.3390/cells8020194
9. Ngkelo A, Meja K, Yeadon M, Adcock I, Kirkham PA (2012) LPS induced inflammatory responses in human peripheral blood mononuclear cells is mediated through NOX4 and Giα dependent PI-3kinase signalling. J Inflamm (Lond) 9(1):1
10. Chen Y, Ji N, Pan S, Zhang Z, Wang R, Qiu Y, Jin M, Kong D (2017) Roburic acid suppresses NO and IL-6 production via targeting NF-κB and MAPK pathway in RAW264.7 cells. Inflammation 40(6):1959–66
11. Cao X, Jin Y, Zhang H, Yu L, Bao X, Li F, Xu Y (2018) The anti-inflammatory effects of 4-((5-Bromo-3-chloro-2-hydroxybenzyl)amino)-2-hydroxybenzoic acid in lipopolysaccharide-activated primary microglial cells. Inflammation 41(2):530–540
12. Hoang LS, Tran MH, Lee JS, Ngo QM, Woo MH, Min BS (2016) Inflammatory Inhibitory Activity of Sesquiterpenoids from *Atractylodes macrocephala* rhizomes. Chem Pharm Bull (Tokyo) 64(5):507–511
13. The State Pharmacopoeia Commission of P.R. China (2005) Pharmacopeia of People's Republic of China. Chemical Industry Press, Beijing
14. Li Y, Yang XW (2014) New eudesmane-type sesquiterpenoids from the processed rhizomes of *Atractylodes macrocephala*. J Asian Nat Prod Res 16(2):123–128
15. Gu S, Li L, Huang H, Wang B, Zhang T (2019) Antitumor, antiviral, and anti-Inflammatory efficacy of essential oils from Atractylodes macrocephala Koidz. Produced with different processing methods. Molecules 24(16):2956

Jin *et al. Applied Biological Chemistry*   (2022) 65:11

Page 13 of 13

16. Ji G, Chen R, Zheng J (2014) Atractylenolide I inhibits lipopolysaccharide-induced inflammatory responses via mitogen-activated protein kinase pathways in RAW264.7 cells. Immunopharmacol Immunotoxicol 36(6):420–5

17. More S, Choi DK (2017) Neuroprotective role of atractylenolide-I in an in vitro and in vivo model of Parkinson's disease. Nutrients 9(5):451

18. Cheng Y, Chen T, Yang X, Xue J, Chen J (2019) Atractylon induces apoptosis and suppresses metastasis in hepatic cancer cells and inhibits growth in vivo. Cancer Manag Res 11:5883–5894

19. Li J, Li F, Xu Y, Yang W, Qu L, Xiang Q, Liu C, Li D (2013) Chemical composition and synergistic antioxidant activities of essential oils from *Atractylodes macrocephala* and *Astragalus membranaceus*. Nat Prod Commun 8(9):1321–4

20. Liu J, Chen X, Yue C, Hou R, Chen J, Lu Y, Li X, Li R, Liu C, Gao Z, Li E, Li Y, Wang H, Yan Y, Li H, Hu Y (2015) Effect of selenylation modification on immune-enhancing activity of *Atractylodes macrocephala* polysaccharide. Int J Biol Macromol 2015(72):1435–1440

21. Li Y, Liu J, Yang XW (2013) Four new eudesmane-type sesquiterpenoid lactones from atractylenolide II by biotransformation of rat hepatic microsomes. J Asian Nat Prod Res 15(4):344–356

22. Yoichi N, Yohya W, Takako S, Seto T (1976) Studies on the components of atractylodes. I. New sewquiterpwnoids in the rhizome of *Artactylodes lancea* De candolle. Yakugaku Zasshi 96(11):1089–93

23. Li Y, Yang XW (2013) Five new eudesmane-type sesquiterpenoid lactones biotransformed from atractylenolide I by rat hepatic microsomes. Fitoterapia 85:95–100

24. Chen LG, Jan YS, Tsai PW, Norimoto H, Michihara S, Murayama C, Wang CC (2016) Anti-inflammatory and anti-nociceptive constituents of *Atractylodes japonica* Koidzumi. J Agric Food Chem 64(11):2254–2262

25. Ding HY, Liu MY, Chang WL, Lin HC (2005) New sesquiterpenoids from the rhizomes of *Atractylodes macrocephala*. Chin Pharm J 57:37–42

26. Wang HX, Liu CM, Liu Q, Gao K (2008) Three types of sesquiterpenes from rhizomes of *Atractylodes lancea*. Phytochemistry 69:2088–2094

27. Guo H, Diao QP, Zhang B, Wang WF, Wang LX (2018) Chemical constituents from *Pholiota nameko*. Zhongyaocai 41:350–352

28. Kamto ELD, Ngono DSB, Mbing JN, Atchadé ADT, Pegnyemb DE, Westhuizen JHVD (2014) An aromatic amide C-glycoside and a cyclitol derivative from stem barks of *Piper guineense* Schum and Thonn (Piperaceae). Phytochem Lett. 10:11–12

29. Ruth J, Ferdinand B, Siegmar S (1979) Weitere acetylenverbindungen aus *Centaurea ruthenica*. Phytochemistry 18:829–837

30. Chen ZL (1987) The acetylenes from *Atractylodes macrocephala*. Planta Med 53(5):493–494

31. Jerezano A, Jiménez F, Cruz MC, Montiel LE, Delgado F, Tamariz J (2011) New approach for the construction of the coumarin frame and application in the total synthesis of natural products. Helv Chim Acta 94:185–198

32. Zhu TF, Chen JJ, Sun QW, Yan ZH (2017) Chemical constituents from *Picrorhiza scrophulariiflora*. Zhongcaoyao 48:263–265

33. Xiao SJ, Guo DL, He DH, Xia B, Chen F, Ding LS, Zhou Y (2016) Chemical constituents of *Clematoclethra scandens* subsp. actinidioides. Zhongcaoyao 47:383–7

34. Nakatani N, Kayano S, Kikuzaki H, Sumino K, Katagiri K, Mitani T (2000) Identification, quantitative determination, and antioxidative activities of chlorogenic acid isomers in prune (*Prunus domestica* L.). J Agric Food Chem 48(11):5512–6

35. Carnat A, Heitz A, Fraisse D, Carnat AP, Lamaison JL (2000) Major dicaffeoylquinic acids from *Artemisia vulgaris*. Fitoterapia 71(5):587–589

36. Ma HY, Sun Y, Lu AL, Chen G, Wu HH, Pei YH (2010) Isolation and identification of chemical constituents from *Artemisia capillaries* Thunb. Chin J Med Chem 20:61–63

37. Coleman JW (2001) Nitric oxide in immunity and inflammation. Int Immunopharmacol 1(8):1397–1406

38. Sharma JN, Al-Omran A, Parvathy SS (2007) Role of nitric oxide in inflammatory diseases. Inflammopharmacology 15(6):252–259

39. Guix FX, Uribesalgo I, Coma M, Muñoz FJ (2005) The physiology and pathophysiology of nitric oxide in the brain. Prog Neurobiol 76(2):126–152

40. Choudhari SK, Chaudhary M, Bagde S, Gadbail AR, Joshi V (2013) Nitric oxide and cancer: a review. World J Surg Oncol 11:118

41. Cohrt KO (2018) Macrophages and microglia—same but different! https://www.tempobioscience.com/blog/macrophages-and-microglia-same-but-different-part-i. Accessed 13 Jan 2018

42. Guasti L, Squizzato A, Moretto P, Vigetti D, Ageno W, Dentali F, Maresca AM, Compiotti L, Grandi AM, Passi A (2017) In vitro effects of Apixaban on 5 different cancer cell lines. PLoS ONE 12(10):e0185035

43. Andreasson K (2010) Emerging roles of PGE_2 receptors in models of neurological disease. Prostaglandins Other Lipid Mediat 91(3–4):104–112

44. Ricciotti E, FitzGerald GA (2011) Prostaglandins and inflammation. Arterioscler Thromb Vasc Biol 31(5):986–1000

45. Kawahara K, Hohjoh H, Inazumi T, Tsuchiya S, Sugimoto Y (2015) Prostaglandin E2-induced inflammation: relevance of prostaglandin E receptors. Biochim Biophys Acta 1851(4):414–421

46. Zhang JM, An J (2007) Cytokines, inflammation, and pain. Int Anesthesiol Clin 45(2):27–37

47. Kuspa T, Horacek JM, Jebavy L (2012) The role of cytokines in acute myeloid leukemia: a systematic review. Biomed Pap Med Fac Univ Palacky Olomouc Czech Repub 156(4):291–301

48. Blantz RC, Munger K (2002) Role of nitric oxide in inflammatory conditions. Nephron 90(4):373–378

49. Förstermann U, Sessa WC (2012) Nitric oxide synthases: regulation and function. Eur Herat J 33(7):829–837

50. Ying L, Hofseth LJ (2007) An emerging role for endothelial nitric oxide synthase in chronic inflammation and cancer. Cancer Res 67(4):1407–1410

51. Wu X, Gao H, Sun W, Yu J, Hu H, Xu Q, Chen X, Nepetoidin B (2017) a natural product, inhibits LPS-stimulated nitric oxide production via modulation of iNOS mediated by NF-κB/MKP-5 pathways. Phytother Res 31(7):1072–1077

52. Sales KJ, Jabbour HN (2003) Cyclooxygenase enzymes and prostaglandins in pathology of the endometrium. Reproduction 126(5):559–567

53. Williams CS, Mann M, DuBois RN (1999) The role of cyclooxygenases in inflammation, cancer, and development. Oncogene 18(55):7908–7916

54. Morita I (2002) Distinct functions of COX-1 and COX-2. Prostaglandins Other Lipid Mediat 68–69:165–175

55. Simon LS (1999) Role and regulation of cyclooxygenase-2 during inflammation. Am J Med 106(5B):37S-42S

56. Liu T, Zhang L, Joo D, Sun SC (2017) NF-κB Signaling in inflammation. Signal Transduct Target Ther 2:17023

57. Christian F, Smith EL, Carmody RJ (2016) The regulation of NF-κB subunits by phosphorylation. Cells 5(1):12

58. Giridharan S, Srinivasan M (2018) Mechanisms of NF-κB p65 and strategies for therapeutic manipulation. J Inflamm Res 11:407–419

59. Lawrence T (2009) The Nuclear Factor NF-kappaB Pathway in Inflammation. Cold Spring Harb Perspect Biol 1(6):a001651

60. Viatour P, Merville MP, Bours V, Chariot A (2005) Phosphorylation of NF-kappaB and IkappaB proteins: implications in cancer and inflammation. Trends Biochem Sci 30(1):43–52

61. Shih RH, Wang CY, Yang CM (2015) NF-kappaB signaling pathways in neurological inflammation: a mini review. Front Mol Neurosci 8:77

62. Kyriakis JM, Avruch J (2012) Mammalian MAPK signal transduction pathways activated by stress and inflammation: a 10-year update. Physiol Rev 92(2):689–737

63. Ci X, Ren R, Xu K, Li H, Yu Q, Song Y, Wang D, Li R, Deng X (2010) Schisantherin A exhibits anti-inflammatory properties by down-regulating NF-kappaB and MAPK signaling pathways in lipopolysaccharide-treated RAW 264.7 Cells. Inflammation 33(2):126–36

64. Liu Y, Shepherd EG, Nelin LD (2007) MAPK phosphatases—regulating the immune response. Nat Rev Immunol 7(3):202–212

Publisher's Note